CFD Letters

Journal homepage:
https://semarakilmu.com.my/journals/index.php/CFD_Letters/index
ISSN: 2180-1363

Meteotsunami Impact in Indonesia due to the Shockwave of the Hunga Tonga Volcanic Eruption on January 15, 2022

Januar Arifin[1], Mohammad Syamsu Rosid[2*]

[1] Agency for Meteorology Climatology and Geophysics (BMKG), Jakarta 10610, Indonesia
[2] Department of Physics, FMIPA Universitas Indonesia, Depok 16424, Indonesia

ARTICLE INFO

Article history:
Received 9 July 2024
Received in revised form 10 August 2024
Accepted 12 September 2024
Available online 31 October 2024

Keywords:
Meteotsunami; volcanic eruption; shockwave; Proudman resonance

ABSTRACT

This paper presents the impact of a meteotsunami resulting from the shockwave of the underwater volcanic eruption of Hunga Tonga–Hunga Ha'apai (HTHH) on January 15, 2022.The tsunami was detected in various locations in Indonesia through a network of water level sensors monitored by the Agency for Meteorology Climatology and Geophysics (BMKG). The tsunami wave heights varied significantly and exhibited a non-linear relationship with the distance from the volcano. The heights of detected tsunami ranged from 2.8 to 22.6 cm, with the highest recorded at the water level sensor south of Java Island. The heights of waves are believed influenced by Proudman resonance in the Indian Ocean waters beside the local amplification effect. The average period of the tsunami waves was approximately 40 minutes, exceeding five days. The tsunami was triggered by the coupling effect between the shockwave with a velocity of 312 m/s and the sea surface. The air pressure anomalies due to the shockwave ranging from 1.2 to 2.2 hPa. Throughout Indonesian waters, this meteotsunami phenomenon did not have a significant impact.

1. Introduction

Meteotsunami is a natural phenomenon that can cause serious damage in many regions around the world. It is a rare event that can be global in some cases. Meteotsunami is a large wave that appears in the sea due to rapid changes in air pressure. It is a type of tsunami triggered by changes in atmospheric pressure, wind or other air disturbances [1]. Certain regions might face significant damage if hit by a meteotsunami, such as in the case of the Menorca meteotsunami in Spain on June 15, 2006. The high waves reached 4–5 m and caused damage to about 100 boats, with thirty-five of them sinking in the Ciutadella port [2]. The weather phenomenon occurring in the Balearic Islands leads to a sudden atmospheric pressure surge that interacts with the sea surface in that location, triggering such high waves [1, 2].

Meteotsunami can be caused not only by weather factors but also by the propagation of shockwaves or Lamb waves caused by large volcanic eruptions that disturb atmospheric stability and interact with the sea surface. One of the most notable cases of such was a meteotsunami in Indonesia

* *Corresponding author.*
E-mail address: syamsu.rosid@ui.ac.id (Mohammad Syamsu Rosid)

https://doi.org/10.37934/cfdl.17.4.136152

caused by the eruption of Krakatoa in 1883 in the Sunda Strait, which had a global impact [3]. The eruption resulted in a meteotsunami wave that reached distant locations, including Europe and the United States, with a duration of up to nine days [4]. A similar meteotsunami generation event on a smaller scale is the meteotsunami event recorded in the Pacific Ocean due to the eruption of the Bezymianny volcano in Kamchatka, Alaska, on March 30, 1956 [3]. The shockwaves from the powerful volcanic eruption, located more than 60 km inland from the coastline, were able to generate small meteotsunami waves recorded in various locations across the Pacific with a maximum amplitude reaching 30 cm [5].

Recently, the world witnessed a spectacular worldwide volcanic meteotsunami event, regarded as one of the most powerful since the Krakatoa volcano eruption-induced meteotsunami in 1883. This meteotsunami occurred on January 15, 2022, and was caused by the underwater volcanic eruption of Hunga Tonga–Hunga Ha'apai (HTHH), which is regarded as the most powerful eruption event of the twenty-first century [6]. The volcano erupted dramatically, forming a gigantic atmospheric air column with a height of up to 30 kilometres [7]. This huge volcanic explosion, situated in the middle part of the Pacific Ocean as shown in Figure 1(a), obliterated a volcanic deposit island as in Figure 1(b), leaving behind two small islands: Hunga Tonga on the southwest side and Hunga Ha'apai on the northeast side as in Figure 1(c).

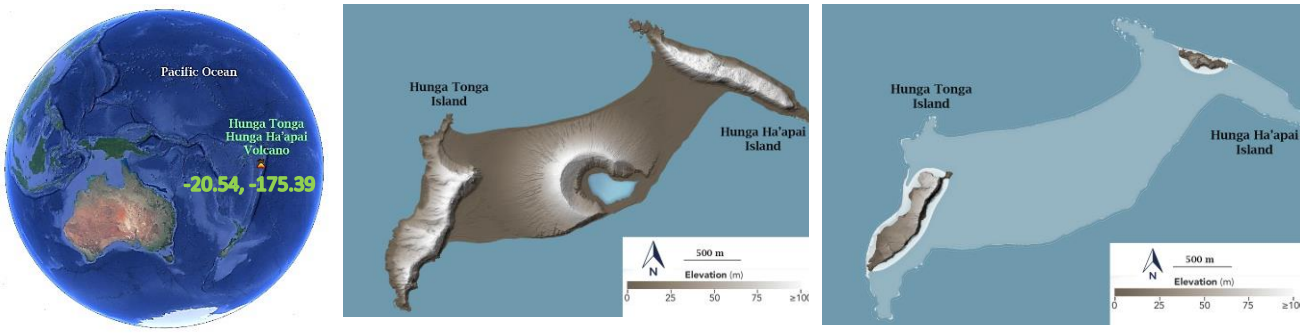

(a) (b) (c)

Fig. 1. (a) Location of the HTHH volcano in the middle part of the Pacific Ocean (b) the body of the HTHH volcano before the eruption on 15 January 2022 and (c) water conditions where the body of the HTHH volcano disappeared after the eruption on January 15, 2022 leaving the two initial islands of Hunga Tonga in the southwest and Hunga Ha'apai in the northeast [8]

The eruption of HTHH resulted in a series of direct tsunami waves propagating through the waters in various coastal areas of the Pacific Ocean. These waves posed a threat of tsunamis at both local and regional scales especially in Pacific Region. The first recorded tsunami wave was observed at 04:27 UTC at the Nuku'alofa Tide Gauge station in Tongatapu, with a height of 1.2 m [9]. At a regional scale, Pacific Tsunami Warning Center (PTWC) reported that this direct tsunami was observed on both the tide gauge network and Deep-ocean Assessment and Reporting of Tsunamis (DART) Buoys, with the largest waves from 1 to 2 m at various points across the Pacific Ocean [10]. The most severe damage from this direct tsunami occurred in Tongatapu, where four fatalities were reported [9]. Additional casualties were reported in Peru, with two individuals losing their lives due to drowning caused by these waves [6].

Meteotsunami occurs when volcanoes create air pressure anomalies, such as Lamb waves, that can propagate far in the atmosphere at ultrasonic speed [11]. This mechanism is what led to the global meteotsunami generated by the HTHH volcanic eruption [12]. It results in changes in sea surface height over a significant distance due to impulsive pressure. During the first 45 minutes after the eruption, a substantial air pressure wave propagated, causing a series of meteotsunami to be

detected around the world [13]. Various ground-based and satellite-based equipment systems, including air pressure sensors, seismometers, hydrophones, Global Navigation Satellite System receivers and meteorological satellites, identified this atmospheric wave globally [7]. This meteotsunami was recorded in several places, such as the Pacific [14, 15] and Indian [15] Oceans, Caribbean [16] and Mediterranean [17] Seas. The examples of the detected meteotsunami event in the several mareograms can be seen in Figure 2.

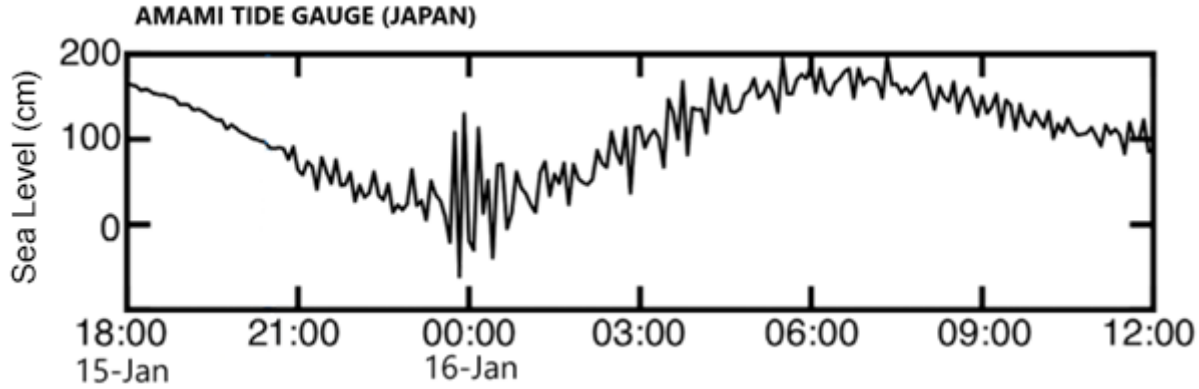

(a)

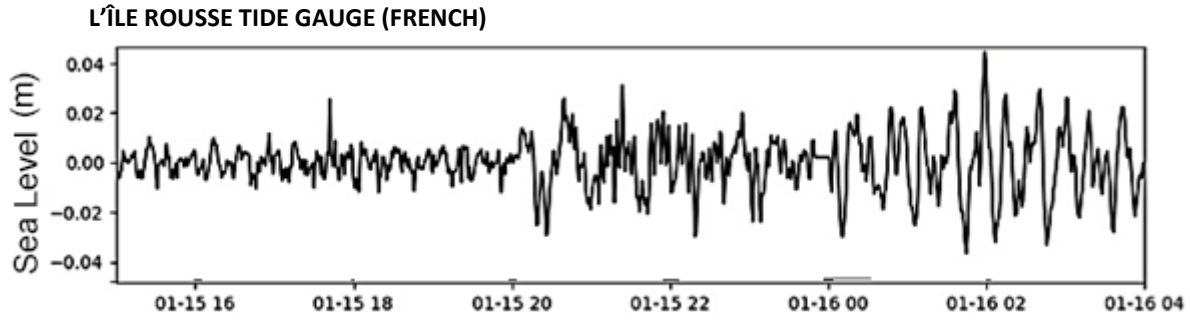

(b)

Fig. 2. (a) The meteotsunami was detected with the largest amplitude of approximately 50 cm in the tide gauge of Amami, Japan due to the eruption of HTHH January 15, 2022 [13] and (b) with a height of approximately 4 cm in the tide gauge of L'Île Rousse, France in the Mediterranean Sea, which is 17,524 km from HTHH volcano [9]

The phenomena of the meteotsunami caused by the eruption of the HTHH volcano has attracted the interest of the global audience, including Indonesia. Although there were no direct tsunami impacts in Indonesia through its waters [19], observations from various parts of the world confirming the presence of meteotsunamis due to the propagation of atmospheric shockwaves caused by the powerful eruption raised the possibility that this meteotsunami may have had effects on Indonesia, despite being located at least 5000 km away. This publication aims to examine the presence of meteotsunamis that occurred in the Indonesian region. This publication will discuss the characteristics and potential impacts of the meteotsunami resulting from the HTHH eruption, assess whether it poses a threat to Indonesia and provide recommendations for mitigation and adaptation to this disaster.

2. Methodology

The data used in this study consisted of recordings from air pressure sensors in the Automatic Weather Stations (AWS) network of BMKG and mareograms from all water level stations monitored by the Indonesia Tsunami Early Warning System (InaTEWS) of BMKG for tsunami detection across Indonesia (as listed in Table 1) during the period of 15–21 January 2022. The monitored water level stations included the tide gauge network operated by the Geospatial Information Agency (BIG), water level AWS and tsunami gauges owned by BMKG, as well as the Inexpensive Device Sea Level (IDSL) operated by the National Research and Innovation Agency (BRIN). All the air pressure sensors in the AWS network use the R.M. Young – 61302 sensor type with a sampling rate of 60 seconds. Three of these sensors are maritime AWS types specifically designed to monitor weather and water levels at ports located in Bitung, North Sulawesi (AWS3010), Padangbai, Bali (AWS3047), and Cilacap (AWS2201). The water level sensors used by the tide gauge and tsunami gauge stations are KRG-10 radar types with a sampling rate of 60 seconds, except for the maritime AWS, which uses VEGAPULS WL 61 radar (sampling rate 60 seconds) and the IDSL, which uses MaxBotix radar (sampling rate 11 seconds).

Table 1
Basic information of Automatic Weather Stations (AWS) and water level station networks of BMKG

No	Station Type, Location & Station Code	Lat. (deg.)	Lon. (deg.)	Air Pressure Sensor	Water Level Sensor
1	AWS Merauke, Papua	-8.47	140.38	●	
2	AWS Jayapura, Papua	-2.54	140.71	●	
3	AWS Timika, Papua	-4.53	136.89	●	
4	AWS Biak, Papua	-1.19	136.10	●	
5	AWS Ambon, Molucca	-3.71	128.09	●	
6	AWS Alor, East Nusa Tenggara	-8.14	124.59	●	
7	AWS Kupang, East Nusa Tenggara	-10.19	123.53	●	
8	AWS Ternate, North Molucca	0.81	127.39	●	
9	AWS Sabu, East Nusa Tenggara	-10.49	121.85	●	
10	AWS Ende, East Nusa Tenggara	-8.85	121.66	●	
11	AWS Bau-Bau, South East Sulawesi	-5.49	122.57	●	
12	AWS Maritime Bitung, North Sulawesi (AWS3010)	1.44	125.18	●	●
13	AWS Sangihe Islands, North Sulawesi	3.69	125.53	●	
14	AWS Ruteng, East Nusa Tenggara	-8.60	120.48	●	
15	AWS Makassar, South Sulawesi	-5.07	119.55	●	
16	AWS Majene, West Sulawesi	-3.55	118.98	●	
17	AWS Maritime Padangbai, Bali (AWS3047)	-8.53	115.51	●	●
18	AWS Denpasar, Bali	-8.75	115.21	●	
19	AWS Banyuwangi, East Java	-8.14	114.40	●	
20	AWS Balikpapan, East Kalimantan	-1.16	116.78	●	
21	AWS Nunukan, North Kalimantan	4.14	117.66	●	
22	AWS Tuban, East Java	-6.82	111.99	●	
23	AWS Sampit, Central Kalimantan	-2.50	112.98	●	
24	AWS Yogyakarta	-7.90	110.05	●	
25	AWS Semarang, Central Java	-6.98	110.38	●	

26	AWS Maritime Cilacap, Central Java (AWS2201)	-7.72	109.02	●	●
27	AWS Pontianak, West Kalimantan	-0.02	109.34	●	
28	AWS Tanjung Priok, Jakarta	-6.12	106.84	●	
29	AWS Merak, Banten	-5.93	106.00	●	
30	AWS Lampung	-5.27	105.18	●	
31	AWS Tanjung Balai Karimun, Riau Islands	0.99	103.44	●	
32	AWS Kerinci, Jambi	-2.09	101.46	●	
33	AWS Pekanbaru, Riau	0.46	101.44	●	
34	AWS Padang, West Sumatra	-0.79	100.29	●	
35	AWS Toba, North Sumatra	2.80	98.79	●	
36	Tide Gauge Jayapura, Papua (JYPR)	-2.55	140.71		●
37	Tide Gauge Tutu Kembong, Molucca (TTKB)	-7.50	131.66		●
38	Tide Gauge Larat, Molucca (LRAT)	-7.15	131.71		●
39	Tide Gauge Biak, Papua (BIAK)	-1.18	136.06		●
40	Tide Gauge Manokwari, West Papua (MWRI)	-0.87	134.08		●
41	Tide Gauge Raja Ampat, West Papua (PAAM)	-0.42	130.80		●
42	Tide Gauge Amahai, Molucca (AMHI)	-3.34	128.92		●
43	Tide Gauge Tulehu, Molucca (TLHU)	-3.59	128.33		●
44	Tide Gauge Ambon, Molucca (AMBN)	-3.64	128.20		●
45	Tide Gauge Pel. Eri, Molucca (PERI)	-3.76	128.12		●
46	Tide Gauge Weda, North Molucca (WEDA)	0.33	127.88		●
47	Tide Gauge Gebe, North Molucca (GEBE)	-0.08	129.43		●
48	Tide Gauge Laiwui, North Molucca (LWUI)	-1.34	127.66		●
49	Tide Gauge Tobelo, North Molucca (TBLO)	1.72	128.02		●
50	Tide Gauge Ternate, North Molucca (TRTE)	0.78	127.39		●
51	Tide Gauge Jailolo, North Molucca (JAIL)	1.06	127.47		●
52	Tide Gauge Kedi, North Molucca (KEDI)	1.68	127.58		●
53	Tide Gauge Kaledupa, South East Sulawesi (KLDP)	-5.51	123.78		●
54	Tide Gauge Maumere, East Nusa Tenggara (MMRE)	-8.62	122.22		●
55	Tide Gauge Melonguane, North Sulawesi (MELO)	4.00	126.68		●
56	Tide Gauge Manado, North Sulawesi (MNDO)	1.50	124.84		●
57	Tide Gauge Torosik, North Sulawesi (TRSK)	0.43	124.28		●
58	Tide Gauge Waingapu, East Nusa Tenggara (WGPO)	-9.64	120.25		●
59	Tide Gauge Tahuna, North Sulawesi (THAN)	3.60	125.50		●
60	Tide Gauge Labuhan Uki, North Sulawesi (LBKI)	0.86	123.94		●
61	Tide Gauge Anggrek, Gorontalo (AGRK)	0.86	122.80		●
62	Tide Gauge Wakai, Central Sulawesi (WKAI)	-0.41	121.87		●
63	Tide Gauge Benete, West Nusa Tenggara (BNTE)	-8.90	116.75		●
64	Tide Gauge Teluk Awang, West Nusa Tenggara (TLAW)	-8.88	116.40		●
65	Tide Gauge LehPa, West Nusa Tenggara (LMBR)	-8.73	116.07		●
66	Tide Gauge Bontang, East Kalimantan (BNTG)	0.18	117.50		●
67	Tide Gauge Sangatta, East Kalimantan (SGTA)	0.47	117.61		●
68	Tide Gauge Sendang Biru, East Java (SBRU)	-8.43	112.68		●
69	Tsunami Gauge Popoh, East Java (POPJI)	-8.26	111.80		●
70	IDSL Prigi, East Java (ID308)	-8.29	111.73		●
71	Tsunami Gauge Pangandaran, West Java (PANJI)	-7.69	108.67		●
72	Tide Gauge Pamayang Sari, West Java (SARI)	-7.77	108.09		●
73	Tide Gauge Pameungpeuk, West Java (PMPK)	-7.66	107.68		●

74	IDSL Pelabuhan Ratu, West Java (ID304)	-6.99	106.54	•
75	IDSL Mentawai Tua Pejat, West Sumatra (ID303)	-2.04	99.59	•
76	Tide Gauge Sirombu, North Sumatra (SIRO)	0.94	97.41	•

The research methodology began with data collection, involving both mareogram data from the sea level network and air pressure data from the BMKG AWS network. Mareogram data were de-trended and de-spiked to remove tidal effects and spike disturbances, followed by a mean sea level correction to obtain residual mareogram data. The de-trended process involves eliminating the tidal effects on the tide gauge record by subtracting the tide gauge data from the tidal model obtained from BIG. The de-spiked process is aimed at removing noise spikes from the tide gauge record by employing a three-point median filter. The mean sea level correction process eliminates signal offsets so that the tide gauge data is centered with the baseline as the mean sea level.

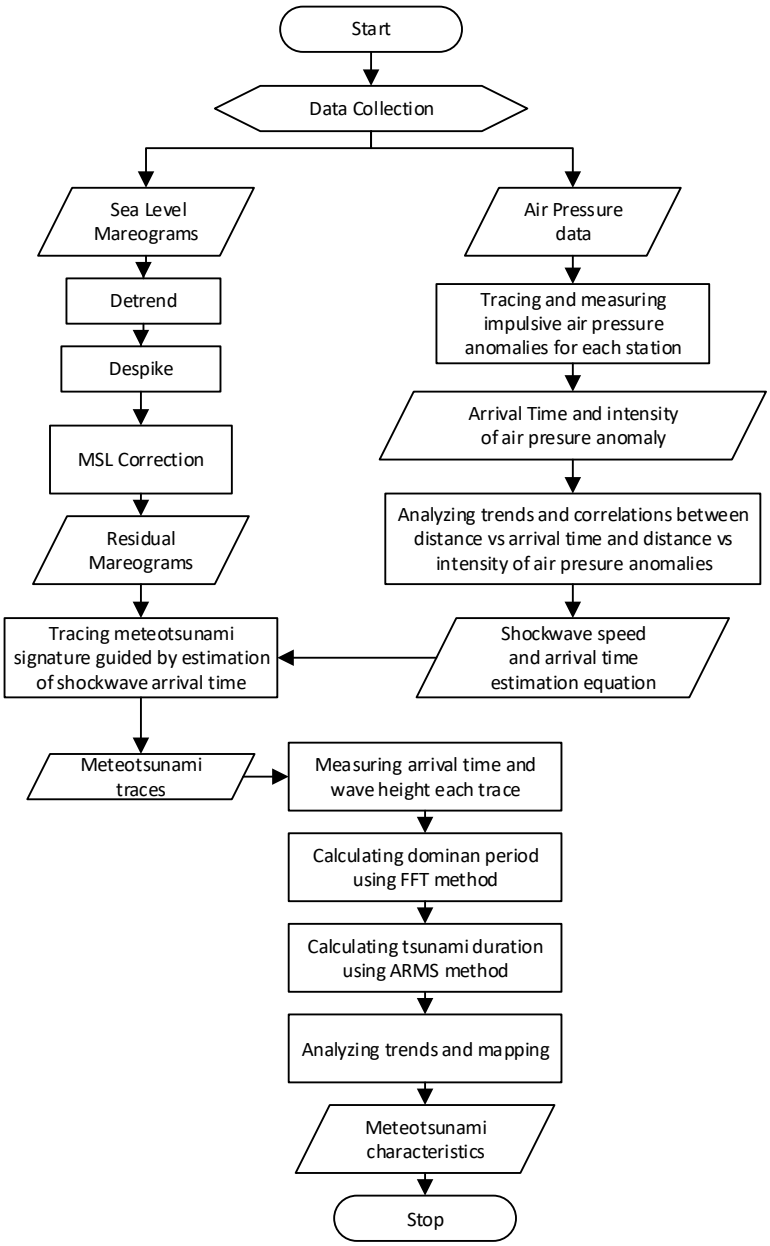

Fig. 3. Flowchart of research methodology

For air pressure data, tracing was conducted for impulse anomalies or sudden air pressure jumps on January 15, 2022, from all air pressure sensors in the BMKG AWS network. The time and value of the pressure anomaly were then analysed for trends to obtain the estimated arrival time of the shockwave and its propagation speed. The estimated shockwave arrival time was subsequently used as a guide to identify the presence of meteotsunami signatures in the residual mareogram data. Each recorded meteotsunami event was identified and characterised by arrival time, wave amplitude, period and duration, which were further used for trend analysis and mapping of their distribution patterns. Dominant meteotsunami periods were determined using spectrum analysis after Fast Fourier Transform (FFT) had been done, and durations were determined using the Averaged-Root-Mean-Square (ARMS) method [20]. The analysis of intensity distribution patterns was carried out with the support of mapping the shockwave propagation direction and the national bathymetry map of Indonesia obtained from BIG to provide an idea of how strong the Proudman resonance was influenced by ocean depth in the generation of meteotsunami waves. The flowchart of methodology can be seen in Figure 3.

Eq. (1) shows the Proudman's formulation [11] for the amplification of sea surface due to pressure movement. It explains the mechanism of tsunami amplification during this process:

$$\eta = \frac{c^2 \eta_s}{c^2 - U^2} = \frac{\eta_s}{1 - F_R^2}, \tag{1}$$

Where η is sea surface displacement; $c = \sqrt{gD}$ is tsunami velocity at depth D; U is the speed of the air pressure, $\eta_s = P/\rho g$ and $F_R = U/c$ is the Froude Number; P is the air pressure disturbance; ρ is sea water density and g is gravitational acceleration. The height of meteotsunami waves can effectively amplify when the speed of the air pressure matches the tsunami's velocity in shallow waters (Proudman resonance), which can be expressed in Eq. (2) below as the relationship between η and P_x as a pressure disturbance at distance x:

$$\eta(x) = -\frac{\mathrm{x}}{2\rho g} P_x . \tag{2}$$

The shockwave propagating through the atmosphere is essentially a type of Lamb wave that moves at speed of sound around 310–320 m/s, which is faster than sea waves in shallow waters typically influenced by the parameter $\sqrt{gD}$ [21].

Meteotsunami waves that propagate towards the coast also experience amplification and changes in wavelength caused by the shoaling effect [14]. According to Green's law for waves in shallow water, the meteotsunami wavelength λ_{local} calculated at a given water depth at the water level sensor, as follows [22]:

$$\lambda_{local} = T\sqrt{gD_{local}} \qquad \text{for } \frac{D_{local}}{\lambda_{local}} < 0.04 \tag{3}$$

Where D_{local} = given water depth at the water level sensor. We can get wavelength calculated at a given offshore λ_0 where the maximum Proudman's resonance occured, so that:

$$\lambda_0 = Tc \tag{4}$$

Then,

$$K_s = \left[(\lambda_{local}/\lambda_0)(1 + \frac{2kD_{local}}{\sinh 2kD_{local}})\right]^{-1/2} \quad (5)$$

Where, $k = 2\pi/\lambda_{local}$ and K_s = shoaling coefficient. Finally we can get estimation of offshore wave height of meteotsunami H_0:

$$H_0 = \frac{H_{local}}{K_s} \quad (6)$$

Where H_{local} = measured meteotsunami wave height at the water level sensor.

3. Results

3.1 Air Pressure Anomaly

According to the air pressure recordings from the AWS network of BMKG on January 15, 2022, over a 24-hour period, there was an extreme air pressure spike observed in 35 AWSs across Indonesia; some examples are shown in Figure 4. These spikes exhibited identical and coherent patterns concerning the distance from each station to the location of the HTHH volcano. The impulsive air anomalies had a range between 1.2 to 2.2 hPa and lasted for approximately 15 to 20 minutes. The distances of the AWS used ranged of 4929–9683 Km from the HTHH volcano.

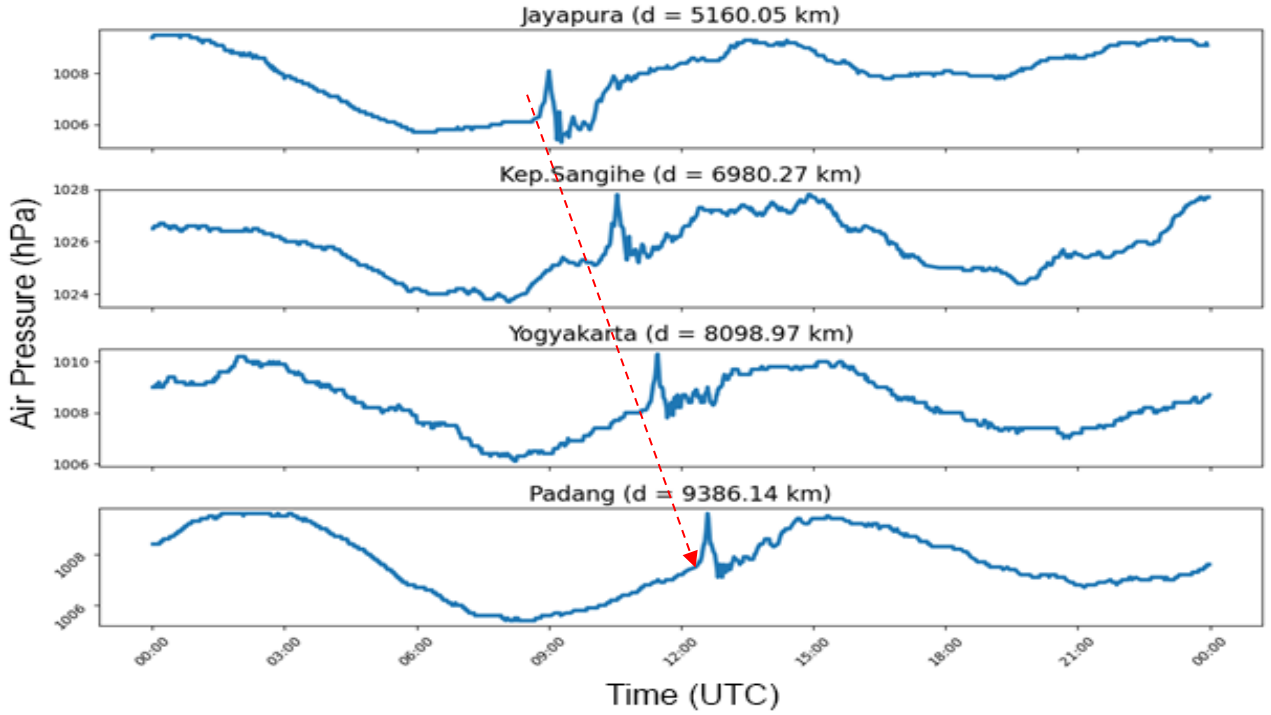

Fig. 4. Examples of the shockwave impulse recordings from the HTHH eruption on January 15, 2022, detected at 35 BMKG AWS in Indonesia

The analysis of the trend in arrival times of air pressure anomalies concerning the distance of each station to the HTHH volcano as shown in Figure 5 reveals a highly strong linear relationship. By taking the initial eruption time at 04:14 UTC [7], the correlation coefficient of the linear regression is 0.998 [7]. Through the gradient of the arrival time trend with respect to distance, the propagation speed of the shockwave is estimated to be approximately 312 m/s.

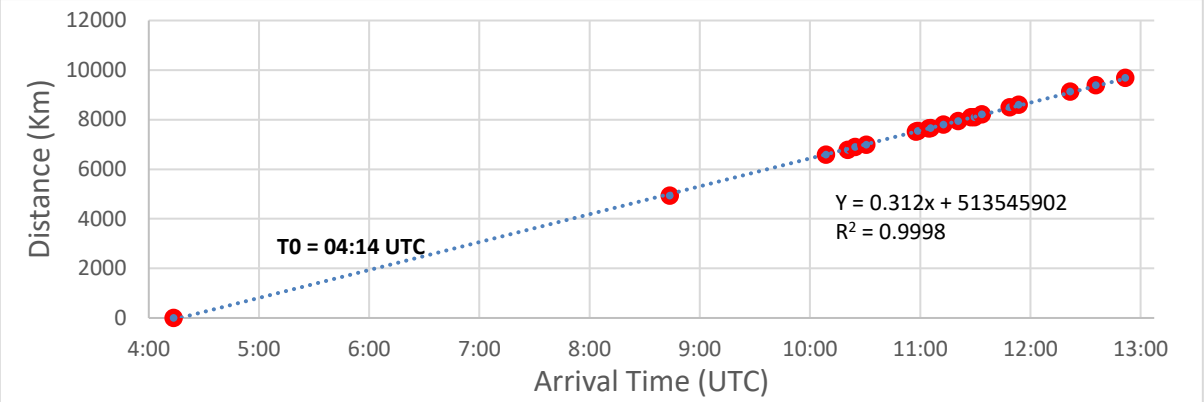

Fig. 5. The red dots represent the observation points of air pressure plotted against the recorded time of air pressure anomalies relative to the distance to HTHH Volcano. They indicate a strong linear relationship between the two variables associated with the propagation of the shockwave resulting from the eruption on January 15, 2022

The characteristics of air pressure anomalies in Indonesia due to the propagation of the HTHH eruption's shockwave are consistent with similar anomalies detected in the air pressure measurement networks in Japan (at over 7000 km from HTHH) at that time, with both exhibiting the same speed of approximately 312 m/s [14]. This suggests an association of shockwave propagation with relatively homogeneous air characteristics across different locations. The strong correlation value between the arrival time trend and the station-to-HTHH distance indicates that the impulsive anomaly signatures present at BMKG AWSs throughout Indonesia provide strong evidence of the air pressure anomalies caused by the propagation of shockwaves from the HTHH eruption that spread in all directions across the Earth.

The analysis of the distance versus air pressure anomaly values at each station as in Figure 6(a) reveals a relatively flat attenuation pattern with a very small gradient of air pressure anomaly concerning distance, approximately -8×10^{-5} hPa/Km. This indicates that, in the propagation of shockwaves across such a vast region of Indonesia, there is no significant attenuation of air pressure. This is further supported by the nearly uniform distribution of air pressure anomalies recorded at AWSs throughout Indonesia as shown in Figure 6(b) below.

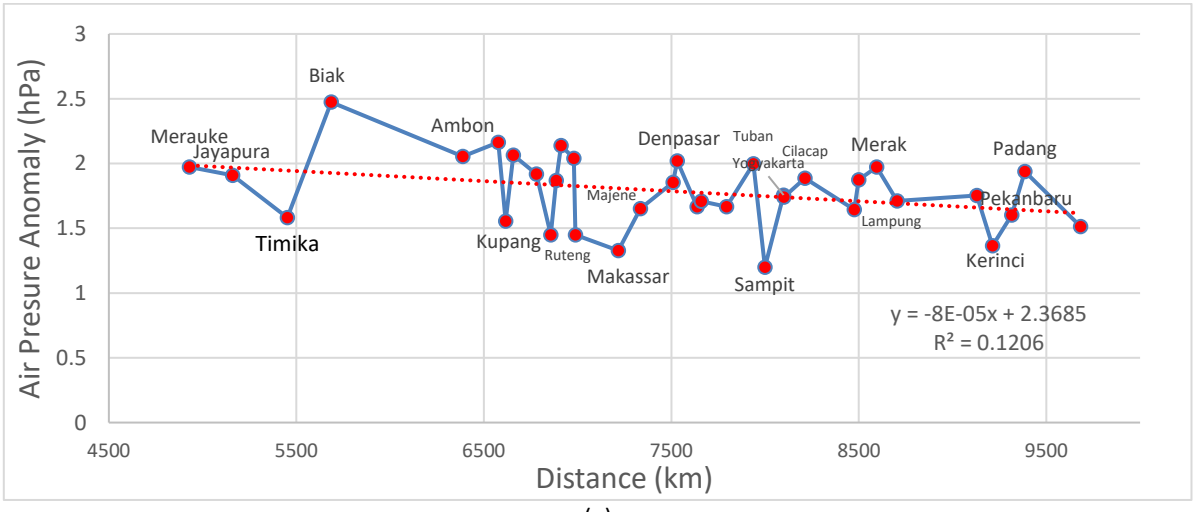

(a)

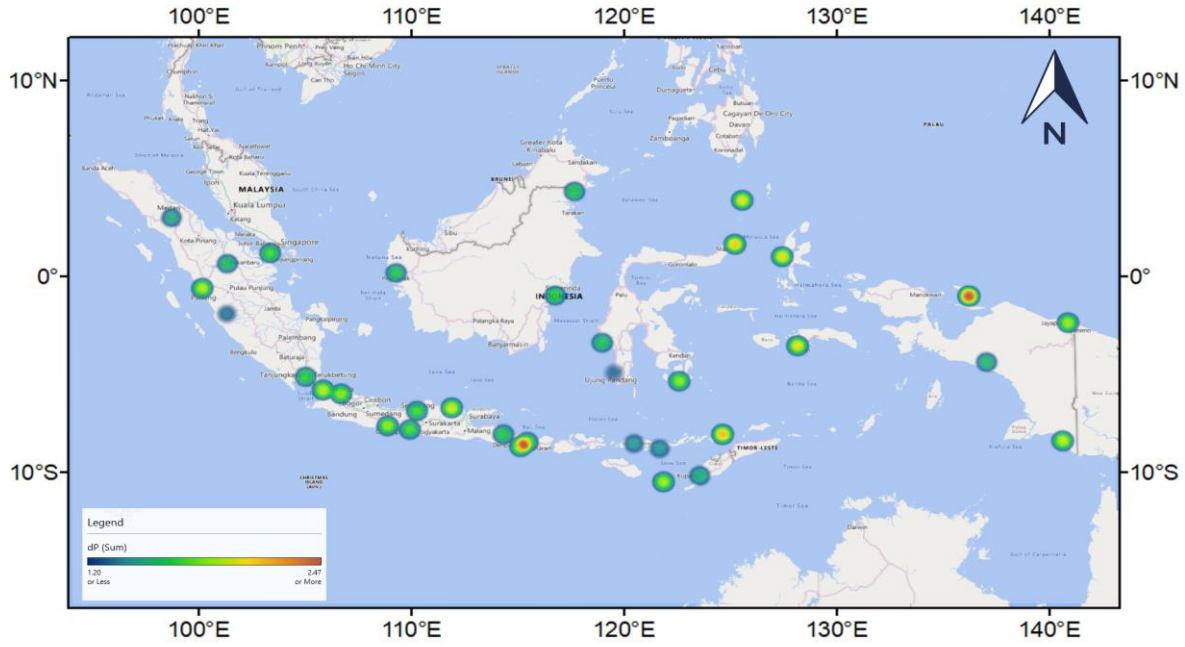

(b)

Fig. 6. (a) The trend of air pressure anomaly along the 35 AWSs throughout Indonesia and (b) the distribution of AWS recorded air pressure anomaly

3.2 Triggered Meteotsunami in Several Locations in Indonesia

Review of sea level data from water level sensors and tide gauge stations near BMKG AWSs were conducted to prove and confirm that the shockwave from the HTHH volcano eruption generated meteotsunami in several places in Indonesia. Through these mareogram data, the presence of sea level anomaly signatures indicating the detection of meteotsunami phenomena was examined.

Tsunami waves have a distinct appearance when recorded by sea-level observation equipment, including meteotsunami. Tsunami waveforms are easily distinguished from the patterns of regular tidal recordings, which generally have much longer periods [23]. The measurement of tsunami height in mareogram recordings is done using the peak-to-peak method. Observers take the highest (maximum) and lowest (minimum) values of the tsunami waveform's amplitudes. Half of the difference between the maximum and minimum heights represents the tsunami amplitude [24].

The height of a meteotsunami cannot be directly measured from mareogram data because the sea level height is still influenced by the tidal elevation at that time. It is essential to separate the meteotsunami waves from the tidal signal, a process referred to as de-tiding. The separation technique involves subtracting the mareogram data values from the daily tidal model at the tide gauge station's location. The difference in data values, known as residual data, represents the meteotsunami signal that is relatively free from the influence of coastal tides. Sometimes, in mareogram recordings, impulsive spikes may appear due to disturbances in the sea level sensor. To remove these spike disturbances under specific circumstances, a de-spiking process is necessary to obtain a more accurate mareogram recording.

Overlaying mareogram data and air pressure data from several sea level and co-located or nearby pressure sensor observation stations revealed that the arrival time of the air pressure impulse was followed almost similarly by the detection of meteotsunami waves at each location as shown in Figure 7. This confirms that the shockwave from the HTHH eruption could generate meteotsunami wave locally with varying heights at several locations in Indonesia.

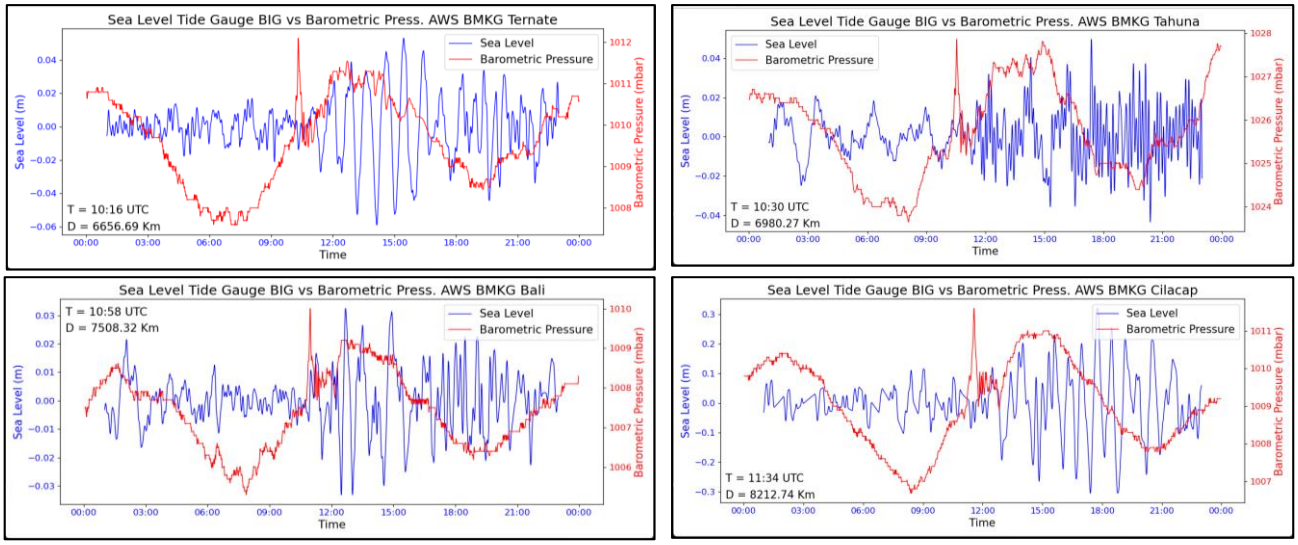

Fig. 7. Examples of the overlaying the air pressure data and sea level mareogram data from the Maritime AWSs or tide gauge stations located near BMKG AWSs on January 15, 2022

Through the regression model equation describing the linear relationship between the arrival time of air pressure anomalies and the distance to the HTHH volcano, it is possible to obtain predicted arrival times of shockwave waves at locations of interest in Indonesia. These predicted arrival times are highly valuable for confirming the existence of meteotsunami waves recorded at various water level stations across Indonesia. By using mareogram data from water level stations, including tide gauge stations owned by BIG, maritime AWS and tsunami gauges by BMKG and IDSL owned by BRIN, the presence of tsunami-like waves recorded on January 15, 2022, was identified. It was confirmed that their arrival times were similar to the predicted arrival times of the HTHH eruption shockwave at each location, as shown in Figure 8 below.

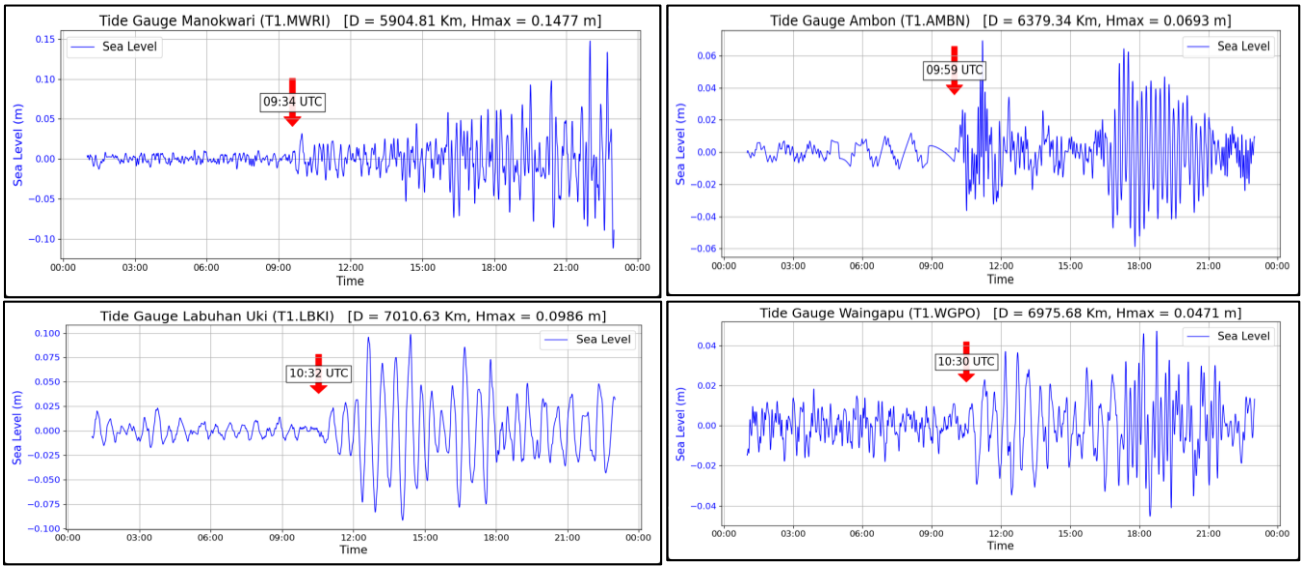

Fig. 8. Examples mareogram recordings from water level stations across Indonesia detected the presence of meteotsunami waves, and the predicted arrival time of the air shockwave (red arrow) confirms the initial meteotsunami wave signature in the mareogram recording (blue colour)

The maximum wave heights recorded for meteotsunami varied, with the lowest being 2.8 cm and the highest reaching 22.6 cm, resulting in an average height of 7.3 cm. This variability demonstrates

that each location experienced a unique maximum height, even though the air pressure anomalies in the Indonesian region exhibited considerable diversity.

In our analytical approach, we employed spectral analysis through the FFT method to scrutinise each mareogram recording in detail. The dominant periods of each meteotsunami recording ranged from 15.57 minutes to 88.09 minutes, with an average period of 40.31 minutes. The spectral analysis of the detected meteotsunami in each water level station can be seen in Figure 9. Based on the average period and velocity of the meteotsunami results, it can be obtained that the wavelength of the meteotsunami formed in the deep sea or offshore in Indonesia is 754,723 km, this is close to what was reported to occur in the Sea of Japan, namely around 600 km [14].

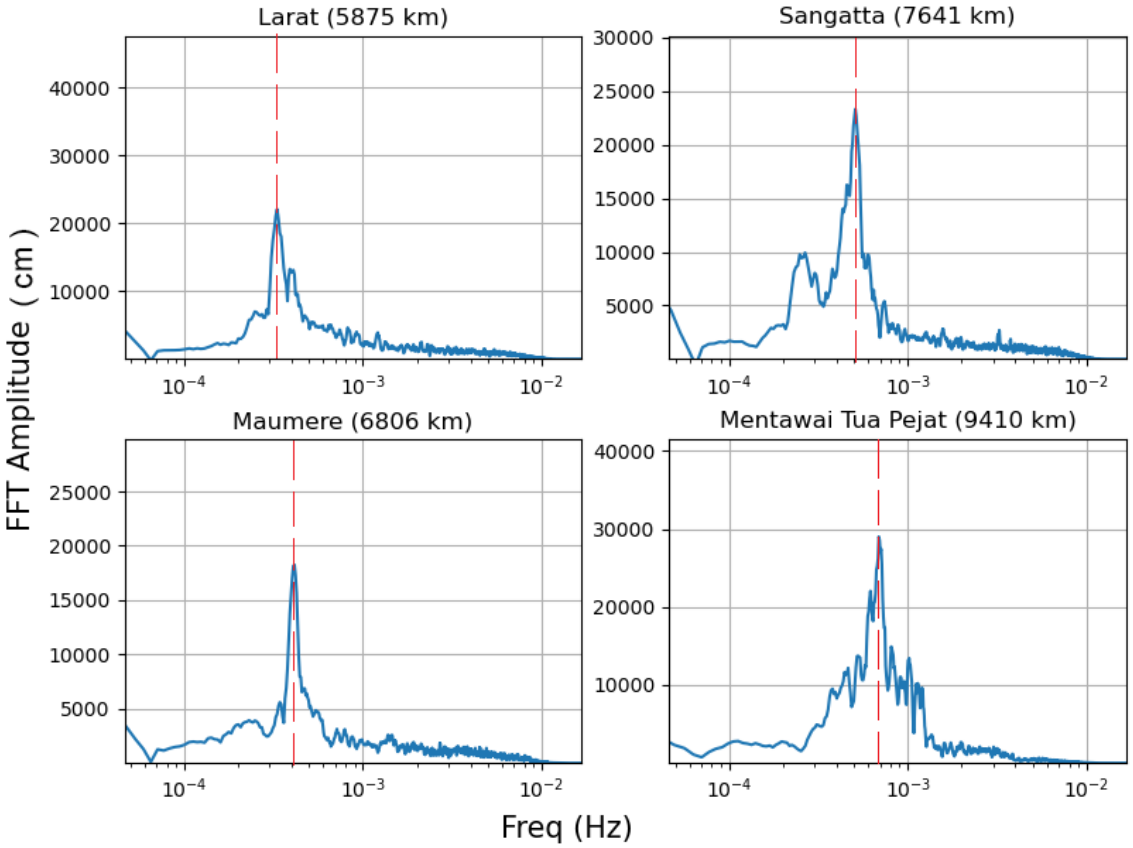

Fig. 9. Examples of the spectrum analysis of meteotsunami signatures related to the HTHH eruption shockwave on January 15, 2022, detected at 44 water level stations in Indonesia

The local wavelength of meteotsunamis recorded on water level sensors ranges from 8,776.16 Km to 49,640.16 Km, with an average of 22,717.85 Km. This variation in wavelength indicates the presence of the shoaling effect phenomenon, which causes the shortening of the wavelength from its original form when first formed offshore. In addition to the wavelength, this phenomenon also causes coastal amplification of the meteotsunami waves as they propagate towards the shore. From all the locations of water level sensors, shoaling coefficients were obtained ranging from 2.76 to 6.56, with an average of 4.33. This variability indicates the complexity of the characteristics of coastal shallows, which vary between each location of the water level sensor. The highest shoaling effect occurs at the Benete water level sensor location in West Nusa Tenggara, while the lowest occurs in Bontang, East Kalimantan.

To assess the magnitude of the Proudman resonance effect, it is necessary to estimate the height of the meteotsunami waves when they form offshore, by disregarding the shoaling effect as described in Eq. (6). The estimation of wave height offshore in the Indonesian region varies, with the

lowest value occurring in deep sea near the Port of Eri, Maluku, at a height of 0.56 cm, and the highest value near the location of Cilacap, Central Java, at a height of 6.08 cm. This is quite reasonable considering the location of Cilacap, situated to the south of Java Island, facing directly towards the Indian Ocean, which has the Java Trench, a sufficiently deep trench contributing to the magnitude of the Proudman resonance effect in forming high meteotsunami waves in deep sea..

The analysis of meteotsunami event durations at each location was carried out using the ARMS method [20]. The recorded meteotsunami events at each location had remarkably long durations, with an average span of approximately five days, as shown in Figure 10. This extended duration of meteotsunami events generated by HTHH has also been documented in the region of Mexico, Central America, which is approximately 9000 km from HTHH [16].

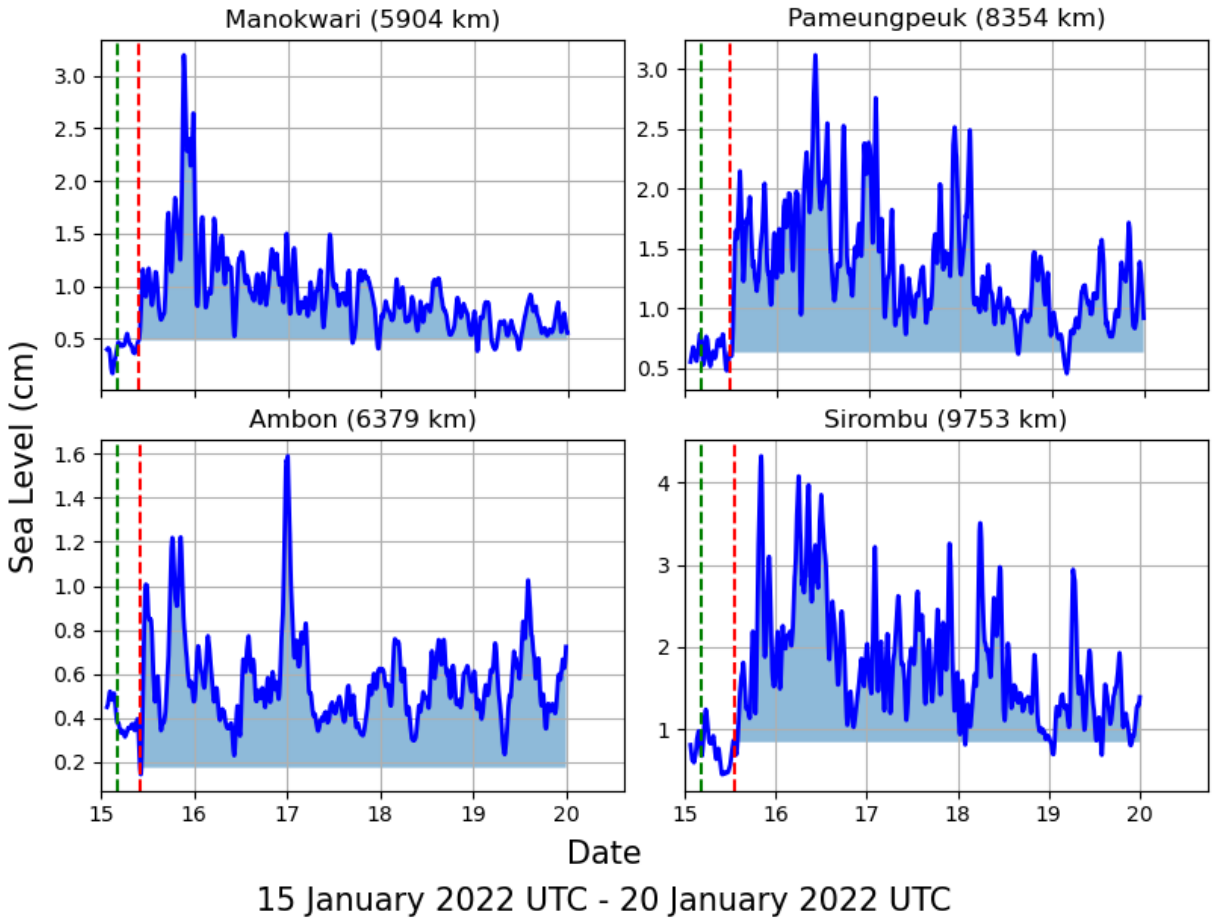

Fig. 10. Examples of the analysis of HTHH meteotsunami durations using the ARMS method

There are reports from the community in the form of video recordings showing the sudden appearance of tidal waves resembling a small meteotsunami on January 15, 2022, at around 19:00 Eastern Indonesia Time (WIT) or 10:00 UTC. This event occurred near the Merah Putih Bridge, along the Ambon Bay coastline in Maluku. The presence of these tsunami-like waves reported by the community aligns in time with the shockwave generated by the HTHH eruption in the air pressure sensor data and the meteotsunami signature in the water level sensor data in Ambon Bay, Maluku.

3.4 Characteristics of the Impact of the HTHH Meteotsunami in Indonesia

The presence of the meteotsunami signature in the mareogram in this case can be traced with the arrival time guide of the impulse shockwave recorded by the nearest water pressure sensor as shown in Figure 7. Almost all the meteotsunami wave arrival times match the impulse shockwave arrival time. However, a slight delay in the recorded arrival time of the meteotsunami wave, which is slower, is due to the decoupling effect between the propagation of atmospheric disturbances and the ocean waves, resulting from shoaling effects as the ocean waves approach shallow waters or the coastline [18, 25].

The tsunami wave has distinctive characteristics compared to regular ocean waves [26], potentially being more dangerous despite not having significant height. Meteotsunami waves generated and reached the shores of Indonesia approximately 4.5 to 8.5 hours after the eruption. These waves recorded a maximum height ranging from 2.8 cm to 22.6 cm, with an average period of about 40 minutes, and persisted for over five days. While categorised as relatively small, evidence from video recordings, suggests that the resulting currents were quite strong when they reached the shores as reported along the coast of Ambon Bay. There were no reports of significant damage caused by these waves in Indonesia.

The meteotsunami waves generated by the HTHH eruption were amplified by the shape and depth of the seafloor along their path, effectively influenced by Proudman resonance at those locations. Meteotsunami heights vary in different locations in Indonesia, but they do not exhibit a strong correlation with distance. A similar pattern is observed in the dominant wave period parameter. The average dominant wave period is 40.31 minutes, in line with the period characteristic of Lamb waves in the atmosphere as their trigger, in the range of 40 minutes [27].

Meteotsunami waves approaching the coast became larger when passing through shallow and narrow areas, such as continental shelves, bays or estuaries. These waves can also resonate with the natural frequencies of enclosed or partially enclosed bodies of water, such as lakes or closed-off bays. Coastal amplification through the this shoaling effect phenomenon also influences the recorded height of meteotsunami waves. The magnitude of the shoaling effect is greatly influenced by the characteristics of the coastal shallows through which the waves pass. Indonesia, being an archipelago with diverse coastal shallow characteristics, results in significant variability in the magnitude of this shoaling effect.

The maximum meteotsunami heights were observed in the South Java, Bali and Nusa Tenggara regions. This is associated with their proximity to the very deep Indian Ocean trench on their southern side, reaching depths of up to 7000 m. It is suspected that significant meteotsunami heights also formed along the coasts of the Banda Sea, which has a depth of around 7500 m, as can be observed through Figure 11. However, the limited number of water level stations and their positions, which are not directly facing the sea, make it challenging to confirm this.

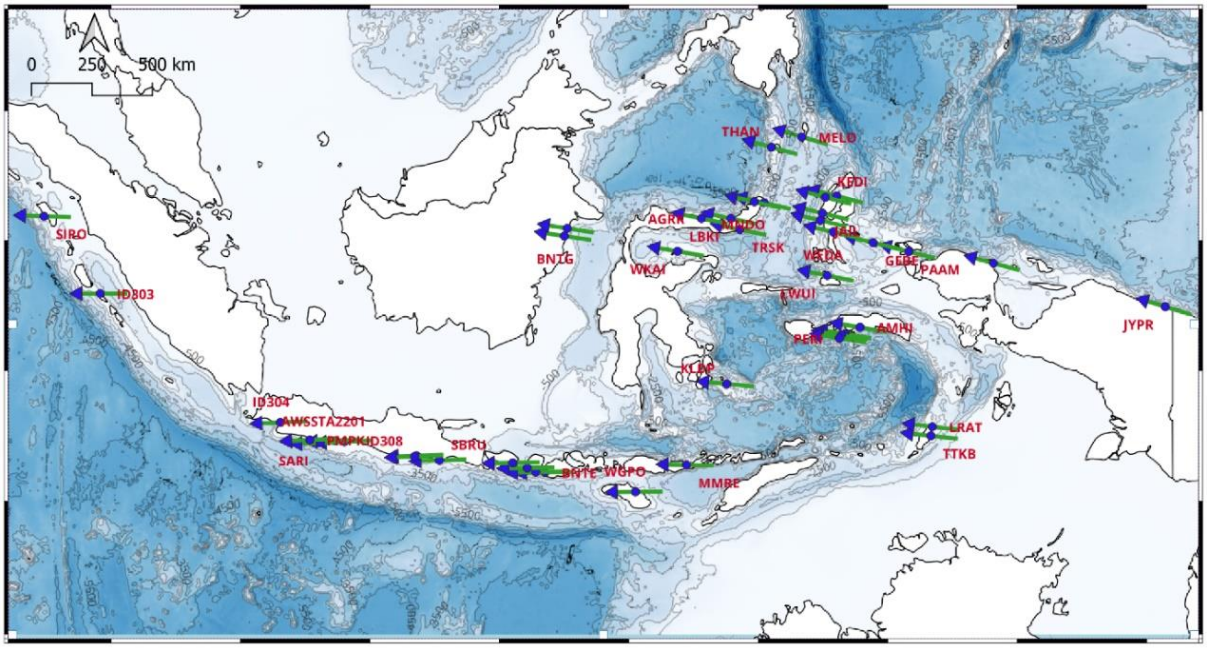

Fig. 11. Bathymetry map and the propagation direction of the shockwave from the HTHH eruption on January 15, 2022, in the Indonesian region

The propagation direction of shockwaves from the HTHH volcano generally enters the Indonesian region from the east to the west. This propagation direction does not seem to significantly influence the maximum height of the meteotsunami that forms. So, the direction of propagation is generally parallel to the coastlines of Nusa Tenggara, Bali and Java, where the highest meteotsunami is observed in Indonesia.

Although the meteotsunami generated by the eruption of HTHH did not cause significant damage in Indonesia, it is crucial for the government, researchers and communities in this region to continue to understand the potential threat of meteotsunami and enhance their preparedness. With the development of improved early warning systems and appropriate education, it is hoped that Indonesia and other vulnerable regions will be better equipped to face potential meteotsunami events in the future.

4. Conclusion

The eruption of the HTHH volcano on January 15, 2022, triggered shockwaves that propagated worldwide. These shockwaves have the potential to generate meteotsunami, even in locations far from the eruption centre. In Indonesia, meteotsunami resulting from this event were detected by a network of water level sensors, with maximum heights varying between 2.8 cm and 22.6 cm. The average period of these tsunami-like wave was approximately 40 minutes, and they persisted for over five days. The meteotsunami height was influenced by the effective occurrence of Proudman resonance in the deep waters of Indonesia and coastal amplification effect as well. The impact of this meteotsunami in Indonesia was not significant, with the maximum effect observed in the southern part of Java Island. However, similar events, even from volcanoes within Indonesia, could occur in the future, potentially on a different scale. This is reminiscent of the historical meteotsunami event caused by the eruption of Krakatoa in 1883, which had relatively significant impacts on locations far from its source. As the next step forward, there is a need for research regarding the early detection of this meteotsunami threat as well as its mitigation efforts.

Acknowledgement
We would like to express our gratitude to all those who have contributed to the success of this study. We also extend our appreciation to the providers of the necessary data sources from BIG, BRIN, and BMKG. In particular, we would like to thank Maulana Putra for his support and guidance in utilizing data from the BMKG Automatic Weather Station (AWS). This research was funded by BMKG through the doctoral scholarship program at the Pusdiklat BMKG.

References

[1] Monserrat, Sebastià, Ivica Vilibić, and Alexander B. Rabinovich. "Meteotsunamis: atmospherically induced destructive ocean waves in the tsunami frequency band." *Natural hazards and earth system sciences* 6, no. 6 (2006): 1035-1051. https://doi.org/10.5194/nhess-6-1035-2006

[2] Jansa, Agustin, Sebastià Monserrat, and Damià Gomis. "The rissaga of 15 June 2006 in Ciutadella (Menorca), a meteorological tsunami." *Advances in Geosciences* 12 (2007): 1-4. https://doi.org/10.5194/adgeo-12-1-2007

[3] Yokoyama, I. "A scenario of the 1883 Krakatau tsunami." *Journal of Volcanology and Geothermal Research* 34, no. 1-2 (1987): 123-132. https://doi.org/10.1016/0377-0273(87)90097-7

[4] Choi, Byung Ho, Efim Pelinovsky, K. O. Kim, and J. S. Lee. "Simulation of the trans-oceanic tsunami propagation due to the 1883 Krakatau volcanic eruption." *Natural Hazards and Earth System Sciences* 3, no. 5 (2003): 321-332. https://doi.org/10.5194/nhess-3-321-2003

[5] Yamashita, Kei, and Taro Kakinuma. "Interpretation of global tsunami height distribution due to the 2022 Hunga Tonga-Hunga Ha'apai volcanic eruption." (2022). https://doi.org/10.21203/rs.3.rs-1761920/v1

[6] Narvaez, Liliana, Joerg Szarzynski, and Zita Sebesvari. "Technical Report: Tonga volcano eruption." (2022). http://dx.doi.org/10.53324/YSXA5862

[7] Matoza, Robin S., David Fee, Jelle D. Assink, Alexandra M. Iezzi, David N. Green, Keehoon Kim, Liam Toney *et al.,* "Atmospheric waves and global seismoacoustic observations of the January 2022 Hunga eruption, Tonga." *Science* 377, no. 6601 (2022): 95-100. https://doi.org/10.1126/science.abo7063

[8] Marcos Pivetta, "Atmospheric Science: From Tonga to Sao Paulo," (2022).

[9] Borrero, Jose C., Shane J. Cronin, Folauhola Helina Latu'ila, Pupunu Tukuafu, Nikolasi Heni, Ana Maea Tupou, Taaniela Kula *et al.,* "Tsunami runup and inundation in Tonga from the January 2022 eruption of Hunga Volcano." *Pure and applied geophysics* 180, no. 1 (2023): 1-22. http://dx.doi.org/10.1007/s00024-022-03215-5

[10] L. Kong, B. Aliaga, 'Ofa Fa'anunu, and A. Gusman, "Hunga-Tonga Hunga-Ha'apai Eruption and Tsunami: Importance of Real-time Sea Level Data for Tsunami Warning Decision-making.," In: *Ocean Data Conference*. *UNESCO*, Sopot (2022).

[11] Proudman, Joseph. "The effects on the sea of changes in atmospheric pressure." *Geophysical Supplements to the Monthly Notices of the Royal Astronomical Society* 2, no. 4 (1929): 197-209. https://doi.org/10.1111/j.1365-246X.1929.tb05408.x

[12] Omira, R., R. S. Ramalho, Jinyoung Kim, Pablo J. González, U. Kadri, J. M. Miranda, F. Carrilho, and M. A. Baptista. "Global Tonga tsunami explained by a fast-moving atmospheric source." *Nature* 609, no. 7928 (2022): 734-740. http://dx.doi.org/10.1038/s41586-022-04926-4

[13] Carvajal, Matías, Ignacio Sepúlveda, Alejandra Gubler, and René Garreaud. "Worldwide signature of the 2022 Tonga volcanic tsunami." *Geophysical Research Letters* 49, no. 6 (2022): e2022GL098153. http://dx.doi.org/10.1029/2022GL098153

[14] Tanioka, Yuichiro, Yusuke Yamanaka, and Tatsuya Nakagaki. "Characteristics of the deep sea tsunami excited offshore Japan due to the air wave from the 2022 Tonga eruption." *Earth, Planets and Space* 74, no. 1 (2022): 61. http://dx.doi.org/10.1186/s40623-022-01614-5

[15] Devlin, Adam T., David A. Jay, Stefan A. Talke, and Jiayi Pan. "The 2022 Tonga Volcanic Tsunami: Lessons from a Global Event." *EGUsphere* 2022 (2022): 1-30. http://dx.doi.org/10.5194/egusphere-2022-925

[16] Ramírez-Herrera, María Teresa, Oswaldo Coca, and Victor Vargas-Espinosa. "Tsunami effects on the Coast of Mexico by the Hunga Tonga-Hunga Ha'apai volcano eruption, Tonga." *Pure and applied geophysics* 179, no. 4 (2022): 1117-1137. http://dx.doi.org/10.31223/X5X33Z

[17] Heinrich, P., A. Gailler, A. Dupont, V. Rey, H. Hébert, and C. Listowski. "Observations and simulations of the meteotsunami generated by the Tonga eruption on 15 January 2022 in the Mediterranean Sea." *Geophysical Journal International* 234, no. 2 (2023): 903-914. http://dx.doi.org/10.1093/gji/ggad092

[18] Sekizawa, Shion, and Tsubasa Kohyama. "Meteotsunami observed in Japan following the Hunga Tonga eruption in 2022 investigated using a one-dimensional shallow-water model." *SOLA* 18 (2022): 129-134. https://doi.org/10.2151/sola.2022-021

[19] CNN, "BMKG: Tsunami Tonga Tak Sampai ke Indonesia," https://www.cnnindonesia.com/teknologi/20220115195425-199-747129/bmkg-tsunami-tonga-tak-sampai-ke-indonesia, (2022).
[20] Heidarzadeh, Mohammad, and Kenji Satake. "Excitation of basin-wide modes of the Pacific Ocean following the March 2011 Tohoku tsunami." *Pure and Applied Geophysics* 171 (2014): 3405-3419. http://dx.doi.org/10.1007/s00024-013-0731-5
[21] Yamada, Masumi, Tung-Cheng Ho, Jim Mori, Yasuhiro Nishikawa, and Masa-Yuki Yamamoto. "Tsunami triggered by the Lamb wave from the 2022 Tonga volcanic eruption and transition in the offshore Japan region." *Geophysical Research Letters* 49, no. 15 (2022): e2022GL098752. http://dx.doi.org/10.1029/2022GL098752
[22] Antoniadis, C. "Experimental verification of wave breaking formulae for obliquely incident waves on mixed and gravel beaches." *International Journal of Oceanography & Aquaculture* 2, no. 1 (2018). http://dx.doi.org/10.23880/IJOAC-16000127
[23] IOC, *Manual on sea level measurement and interpretation. Volume IV - An update to 2006*. , Paris, 2006.
[24] Intergovernmental Oceanographic Commission. "Wave Reporting Procedures for Tide Observers in the Tsunami Warning System." (1988).
[25] Villalonga, Joan, Àngel Amores, Sebastià Monserrat, Marta Marcos, Damià Gomis, and Gabriel Jordà. "Observational study of the heterogeneous global meteotsunami generated after the Hunga Tonga–Hunga Ha'apai Volcano eruption." *Scientific Reports* 13, no. 1 (2023): 8649. http://dx.doi.org/10.1038/s41598-023-35800-6
[26] Hussein, Emad, Farhan Lafta Rashid, Najah Al Maimuri, Ali Basem, and Hayder Ibrahim Mohammed. "Numerical Assessment of Tsunami Forces on Vertical Wall Structures: Impact of Inundation Depth and Incident Fluid Velocity." *CFD Letters* 16, no. 5 (2024): 78-90. https://doi.org/10.37934/cfdl.16.5.7890
[27] Amores, Angel, Sebastian Monserrat, Marta Marcos, Daniel Argüeso, Joan Villalonga, Gabriel Jordà, and Damià Gomis. "Numerical simulation of atmospheric Lamb waves generated by the 2022 Hunga-Tonga volcanic eruption." *Geophysical Research Letters* 49, no. 6 (2022): e2022GL098240. http://dx.doi.org/10.1029/2022GL098240